Results in Optics 7 (2022) 100217

Contents lists available at ScienceDirect

Results in Optics

journal homepage: www.sciencedirect.com/journal/results-in-optics

Design and analysis of highly sensitive prism based surface plasmon resonance optical salinity sensor

Belal Hossain [a,*], Alok Kumar Paul [a], Md. Arefin Islam [a], Md. Faruk Hossain [a], Md. Mahabubur Rahman [b]

[a] Department of Electrical & Electronic Engineering, Rajshahi University of Engineering & Technology, Rajshahi 6204, Bangladesh
[b] Department of Electrical & Computer Engineering, Rajshahi University of Engineering & Technology, Rajshahi 6204, Bangladesh

ARTICLE INFO

Keywords:
Finite element method
Franckeite
Optical sensor
Surface plasmon resonance
Salinity
Seawater

ABSTRACT

This research presents a highly sensitive surface plasmon resonance (SPR) optical salinity sensor based on angular interrogation method for the quantification of salinity and desalination of sea water. The proposed salinity sensor structure composed of prism-silver (Ag)-silicon (Si)-Franckeite-sensing medium. To achieve the best possible performance *i. e.* sensitivity, detection accuracy, and quality factor, the sensor is designed and simulated at different wavelengths of 633 nm, 643.8 nm, 690 nm, 700 nm, and 720 nm. The performance of the sensor has also been optimized for different thickness of Ag layer, Si layer, and no. of layer of 2D franckeite. An enhanced maximum sensitivity of 305 deg./RIU is obtained with detection accuracy 0.41 deg.$^{-1}$ and quality factor 63.92 RIU^{-1}. As the sensor provides high grade of performance, this can be used as a salinity sensor for the desalination of seawater.

1. Introduction

Water salinity plays an important role in scientific research, including chemical and biological analysis, human lives, marine ecosystem protection, mineral prospecting, concrete structures health monitoring, etc. So, the level of salt in seawater must be measured since it has a significant impact on seawater organisms and under sea activities. In the traditional method, water salinity is determined by the electrical conductivity of chloride ions as the conductivity depends on the concentration of chloride ions. Interferences from other contaminating ions, however, impair this measuring procedure (Qian et al., 2018). Due to electrolysis, this method is subjected to corrosion and current instability. In recent years, new salinity characterization methods based on ultrasonography or chemical reactions have been developed. Optical methods are based on the dependence of the refractive index on the concentration of salts in seawater. Nowadays, surface plasmon resonance (SPR) based salinity sensors have piqued researchers' attention in this respect due to several benefits such as compactness, high sensitivity, lightweight, remote sensing, and so forth (Xia et al., 2011).

SPR sensor operates on the basis of the attenuated total reflection (ATR) method. The ATR method uses a total internal reflection (TIR) mechanism, which causes a momentary wave known as surface plasmon wave (SPW). The incident light is guided through the ATR crystal to reflect at least off the internal surface in contact with the sensing sample. This reflection of the incident light beam forms the momentary wave extending into the sensing sample (Pumera, 2011). So, SPR is an optical excitation that produces a momentary electromagnetic wave that propagates along with the metal and dielectric material interface. It can be seen as an electron cloud wave that propagates along the direction of the metal-dielectric interface, through the contact of the freely oscillating photons of the incident light with the electrons on the metal surface (Sharma and Pandey, 2018; Pal et al., 2021); with exponentially decaying electric field in metals and dielectrics. Propagation of the electric field and the metal-dielectric interface highly depend on the dielectric refractive index, thus providing high sensitivity to infinitesimal changes in analyte refractive index. Changes in the concentration of biomolecules caused by chemical reactions cause changes in the refractive index near the sensor surface, which leads to a change in the propagation constant of SPW, thus, a change in SPR frequency (SPRF) and SPR angle take place (Homola et al., 1999). In designing SPR sensors, different plasmonic materials can be used, and some suitable applicants are copper (Cu), Ag, gold (Au), etc. Among those plasmonics materials, Ag has outstanding optical properties, like, small optical

* Corresponding author.
E-mail address: belal@eee.ruet.ac.bd (B. Hossain).

https://doi.org/10.1016/j.rio.2022.100217
Received 24 October 2021; Received in revised form 3 January 2022; Accepted 31 January 2022
Available online 3 February 2022

damping, no interband transfer at visible light frequency, sharper resonance peak, less broad SPR curve, etc. For this reason, it can be a material of choice in designing SPR sensors (Hossain et al., 2022). So, better sensitivity can be achieved through the use of silver as plasmonic material. Au is a preferred material but, it reduces detection accuracy due to its broader resonance curve (Kumar et al., 2020). The high refractive index of Si plays an important role in enhancing sensitivity; Transition Metal Dichalcogenide (TMD) and Si based SPR sensors show the highest sensitivity of 147.88 deg./RIU for the WS_2 layer at 633 nm wavelength (Ouyang et al., 2016). In 2019, Gan et al. proposed a SPR sensor using three layers (about 5.4 nm) of franckeite, the sensitivity obtained as high as 196 deg/RIU, and the corresponding figure of merit (FOM) is 40.29 RIU^{-1} (Gan et al., 2019). Later, Srivastava et al. obtained a sensitivity of 208 deg/RIU, FWHM of 12 deg, quality factor (QF) of 17.33 RIU^{-1} (Srivastava and Prajapati, 2020). In 2020, Raikar et al. proposed a salinity sensor to measure salinity in sea water and the sensor provides a maximum sensitivity of 145 deg./RIU, with detection accuracy (DA) of 0.162 $deg.^{-1}$, and QF of 23.56 RIU^{-1} (Raikwar et al., 2020). Rahman et al. have proposed a SPR biosensor with a sensitivity of 194 deg./RIU with QF is calculated as 34.22 RIU^{-1} for Ag based sensor and for Au coated sensor it is 29.39 RIU^{-1} (Rahman et al., 2020). In 2020, Jia et al, proposed a biosensor with $PtSe_2$ coating of 16 nm having a maximum sensitivity of 165 deg./RIU (Jia et al., 2020). In 2021, Rikta et al. proposed a biosensor having a sensitivity of 96.43 deg./RIU and QF of 12.36 RIU^{-1} (Rikta et al., 2021). Though many materials have been used to model SPR sensors, the recent advancement of two dimensional (2D) nanomaterials has taken great attention. Because of the very unique electronic, optical, and catalytic properties, 2D nanomaterials have been used extensively in sensing applications (Pal et al., 2020). Layered 2D materials such as graphene, blue phosphorene, and Transition metal di-chalcogenides and their heterostructures have been explored by the scientific community to enhance the SPR sensor performance for gas and bio sensing application (Srivastava and Prajapati, 2020; Pal et al., 2020). Recently, various artificial stacking heterostructures like graphene based heterostructure, BlueP/MoS_2 have been reported for SPR based sensing and significant enhancement observed in sensitivity (Hossain et al., 2022; Srivastava and Prajapati, 2019, 2020). The idea of forming van der Waals (vdW) heterostructures (Peng et al., 2016) by integrating various two-dimensional materials breaks the limitation of the restricted properties of single material systems. One approach to produce such heterostructures is to use epitaxially grown materials assembled sheet by sheet (Bae et al., 2010). This method, however, remains challenging and has only been demonstrated for a few van der Waals heterostructures so far (Zhang et al., 2014). Another approach is the manual assembly of individual layers obtained by mechanical exfoliation from bulk and the deterministic placement of one layer on top of another. While the sensitivity of the biosensor based on these artificially designed heterostructure(s) can be high, it is not easy to control the lattice orientations. Consequently, undesired atmospheric adsorbates between the layers occur (Molina-Mendoza et al., 2017). On the other hand, naturally occurring layered minerals such as Franckeite (member of the sulfosalt family), which is alternating stacks of PbS-like pseudotetragonal (Q) layer and SnSe-like pseudohexagonal (H) layer, are found to possess naturally VDW superlattices, and it is free from surface contaminations in contrast to the artificially designed heterostructure(s). In recently, Velický et al. obtained the single layer heterostructure (thickness about 1.8 nm) by mechanical and liquid-phase exfoliation of franckeite (Zhu et al., 2013). Franckeite is a 2-dimensional p-type, air stable material which is a very rare feature in 2D semiconductors, and it can be exfoliated into layers mechanically (Zhu et al., 2013); also it is free from surface contaminations in contrast to the artificially designed heterostructure(s). It has a very narrow band gap of less than 0.7 eV. Due to its narrow band gap and its naturally occurring Vander walls heterostucture, it enhances electric field in its interfaces and increases sensitivity. That is why we have used this 2D Franckeite as a guiding layer.

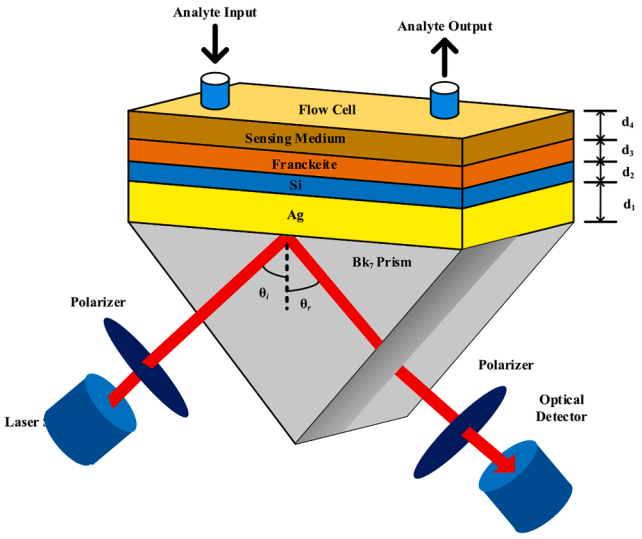

Fig. 1. Schematic design of the proposed sensor with detected light road arrangement.

One of the most challenging global issues in the 21st century is the scarcity of clean water. Climate change, rapid population growth, and rapid urbanization, directly account for freshwater inadequacy on our planet (Lee et al., 2016). Around half of the world's population lives close to oceans that cover 80% of the earth's water supply. Desalination of seawater seems to unravel the world's water shortage issues, particularly within the zones where ground or spring water isn't accessible (Dutta et al., 2016; Oki and Kanae, 2006; Wang et al., 2017). The ocean provides water, which is about 96.5% of all the earth's water is natural, but not potable due to salinity (Xu et al., 2019). Salinity is defined as the concentration of dissolved mineral salts present in waters and soils. Salinity also affects coping agriculture (Elimelech, 2006). The average salinity of standard seawater is 35% at 0 °C (Etesami et al., 2019; Adamo et al., 2015). For water to be taken as a drink, its salinity must be reduced because high salinity has an adverse effect on all living organisms. For measuring the salinity of seawater, different methods are used like conductivity sensor, refractometry sensor. Based on the measurement of the refractive index of seawater (Shannon et al., 2009); it has been shown that the absolute salinity can be accurately assessed because the refractive index of seawater is directly related to the medium density (ρ). In point of the fact that all the physical properties of seawater are derived from salinity (S), pressure (P) and temperature (T) (Shannon et al., 2009). These can be applied to density with the following equation of International State of Seawater, density, $\rho = f(S, T, P)$ (SCOR/IAPSO, 2007).

As in the SPR sensor, a change in analyte refractive index results in a change of the local refractive index of the sensor surface; this change will eventually change the propagation constant of the SPW, resulting in a shift in the SPR angle. Changing in this parameter (SPR angle) can be used to sense the degree of salinity of seawater. In (Raikwar et al., 2020), Surjeet Raikwar et al. measured the seawater concentration using SPR based salinity sensor. They obtained impressive results. But this can be improved further by incorporating the advancement of 2D materials in bimolecular and environmental element sensing, so the design of highly sensitive sensors becomes easier. Franckeite is a newly synthesized 2D material and can be peeled off into layers (Velický et al., 2017). It is an air-stable material, thus less vulnerable to oxidation, and has a crystalline structure. The energy band gap for franckeite is less than 0.7 eV. These features make it an alternative material for black phosphorous (BP) and graphene. The use of franckeite nanosheet in optoelectronic devices has a pronounced prospective (Velický et al., 2017; Ray et al., 2017).

This research work aims to design an SPR based optical sensor that

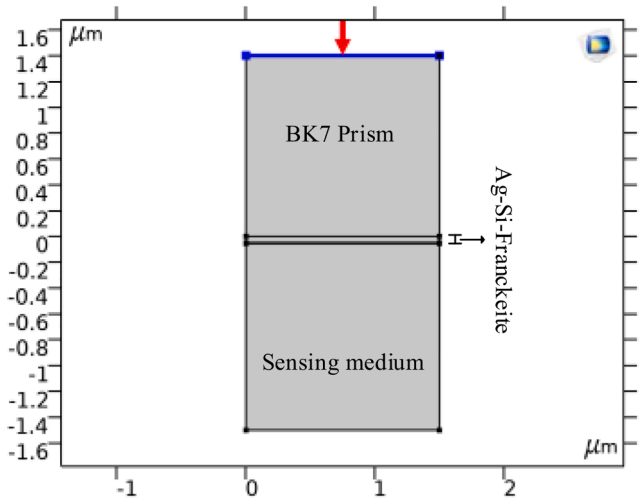

Fig. 2. Generalized configuration of the designed sensor for simulation in COMSOL multiphysics.

can be used as a salinity sensor to sense sea water salinity with a high degree of sensitivity. As temperature and pressure change, the refractive index of seawater also changes (Baker, 2012; Rosen, 1947). This study is done by considering a constant temperature of 20 °C and pressure at 0 kg/cm^2 (Elimelech, 2006).

2. Methodology

2.1. Design consideration and theoretical modeling

Fig. 1 depicts our designed five-layer SPR sensor based on typical Kretschmann configuration. This proposed sensor is prism coupled and uses angular interrogation techniques (Homola et al., 1999). The transverse magnetic (TM) polarized light of different wavelengths incident at one end of the prism and an optical detector receives the reflected optical signal.

Prism is responsible for wave vector matching, which is important for SPR condition to occur. BK7 prism has a low refractive index and, easier to manufacture (Kusko, 2012). Here, prism acts as a base layer. The prism is coated with Ag having a layer thickness, $d_{Ag} = 50$ nm, which in turn covered by a Si layer of thickness, $d_{si} = 5$ nm, and then by a layer of 2D franckeite nanosheet having a thickness, $d_f = L * 1.8$ nm where L represents number of franckeite layers and takes integer values of 0,1,2,3, etc. The refractive indices of different layers are considered as follows. The first layer is BK7 prism, its refractive index can be calculated using Eq. (1).

$$n_{BK7} = \sqrt{1 + \frac{\alpha_1 \lambda^2}{\lambda^2 - \beta_1} + \frac{\alpha_2 \lambda^2}{\lambda^2 - \beta_2} + \frac{\alpha_3 \lambda^2}{\lambda^2 - \beta_3}} \quad (1)$$

where λ is the wavelength of incident light. The values of the constants, α_1, α_2, α_3,β_1 ,β_2 and β_3 are 1.0396121, 0.231792344, 1.0104694, 0.0060006986, 0.020017914, and 103.56065 respectively (Karki et al., 2021). The complex refractive index of Ag layer can be expressed using Drude model, $n_{Ag} = \sqrt{1 - \lambda^2 \lambda_c / \left[\lambda_p^2 (\lambda_c + i\lambda)\right]}$, where collision wavelength, $\lambda_c = 17.614$ μm and plasma wavelength, $\lambda_p = 0.14541$μm (Brahmachari and Ray, 2013). Similarly, the refractive index for Si is taken from this work (Ghosh and Ray, 2015). The complex refractive index of franckeite with L*1.8 nm thickness has been taken from the experimental measurement (Gant et al., 2017). The refractive index of the sensing medium is considered as $n_s = 1.33 + \Delta n_s$; where Δn_s indicates the change in the refractive index of the sensing medium caused by biochemical or bimolecular interaction (Jia et al., 2020).

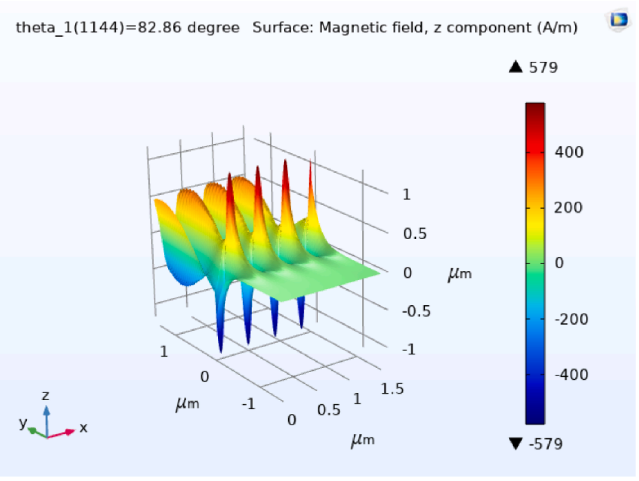

Fig. 3. Propagation of surface magnetic field z component at SPR angle 82.86° (resonance condition) for sample refractive index of 1.33175.

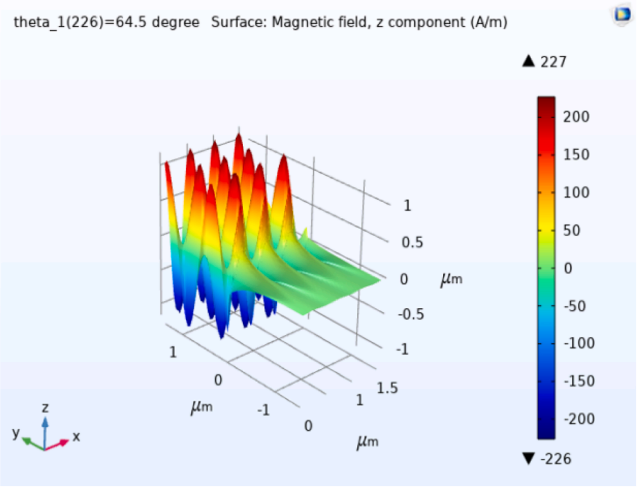

Fig. 4. Propagation of surface magnetic field z component at SPR angle 64.5° (non-resonance condition) for sample refractive index of 1.33175.

In this proposed design, using the Si layer between Ag and franckeite enhances sensitivity as it accelerates the mobility of electrons in franckeite responsible for efficient sensing of analytes at the sensor surface (Kumar et al., 2020).

In our work, saline water with a salinity of 1% to 30% and pure water are considered as analytes in the sensing layer. Refractive indices of saline water correspond to different salinity are taken from (Austin and Halikas, 1976). To simulate our proposed sensor and to evaluate its performance, "COMSOL multiphysics" platform is used with a maximum mesh element size of 0.0581 μm and that of minimum mesh element size of 2.18×10^{-4}μm. Fig. 2 shows that an excitation of TM polarized light is provided on the BK7 prism. We have used a parametric sweep for angular interrogation of the incident light from 60° to 89.98° with an increment of 0.02°. Propagation of z component of surface magnetic field is shown in Fig. 3 at SPR angle of 82.86° (resonance condition) for sample refractive index of 1.33175 and Fig. 4 shows propagation of z component of surface magnetic field at non SPR angle 64.5° (non-resonance condition) for sample refractive index of 1.33175. It is clearly observed from both figures that the distribution of magnetic field is maximum at SPR angle and SPW propagates along metal dielectric interface.

Further, the possibility of practical implementation of the designed

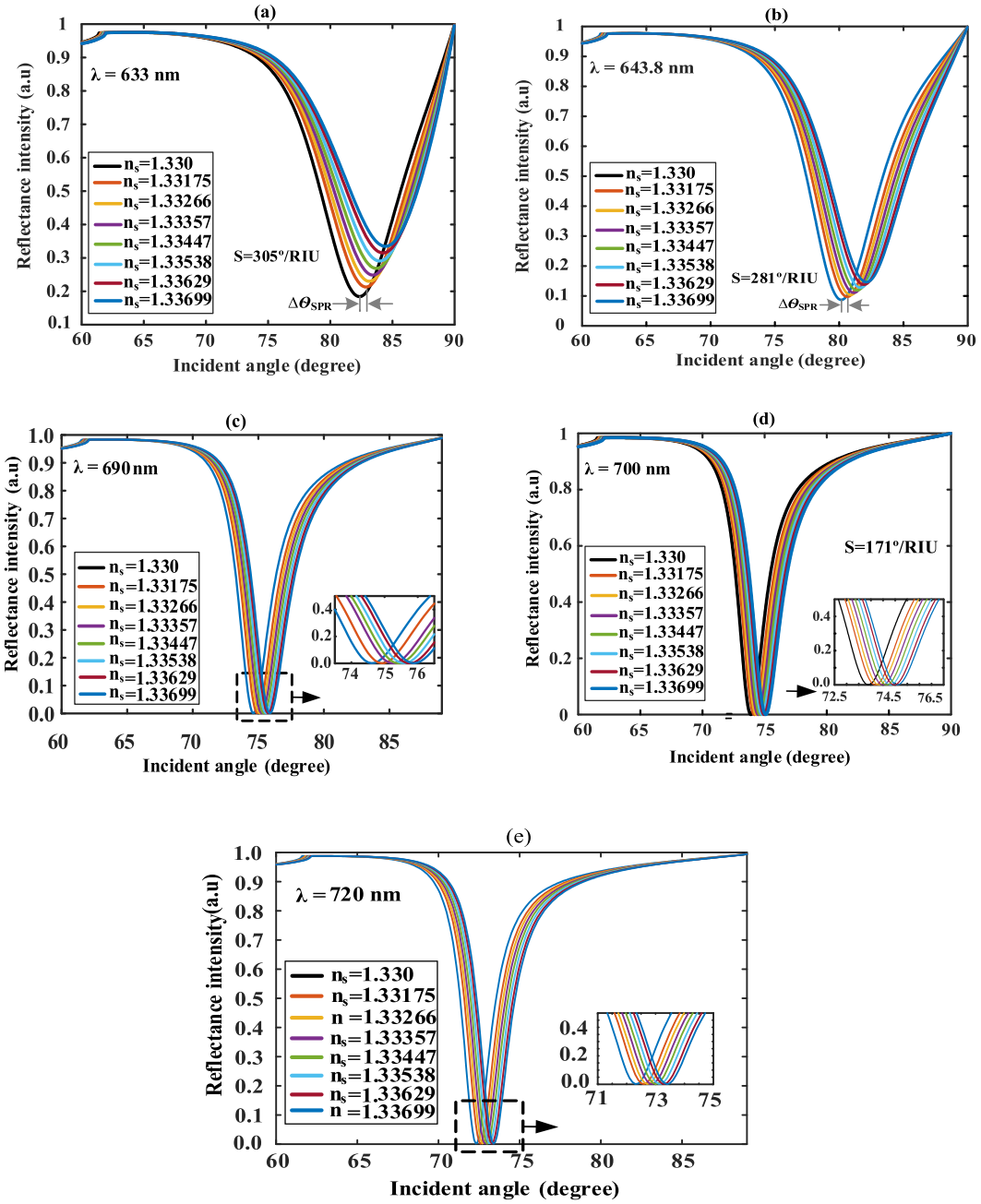

Fig. 5. SPR curves for the proposed sensor at (a) 633 nm, (b) 643.8 nm, (c) 690 nm, (d) 700 nm, and e) 720 nm wavelengths.

sensor and its deposition techniques are discussed. Ag can be deposited on BK7 substrate using the chemical vapor deposition (CVD) method (Boehm et al., 2011). Si can be deposited on top of the Ag layer by the CVD method (Matsumura and Tachibana, 1985). Spin coating deposition technique can be used for franckeite deposition on top of Si layer (Garcia-Basabe et al., 2021). A cuvette can be mounted on the sensor chip to provide a passage for seawater to detect its concentration. The salinity level of seawater can be varied from 1% to 30% at a constant temperature of 20°C, poured into the cuvette, for loading next salinity seawater, the previous concentration was denaturized (Raikwar et al., 2020).

2.2. Mathematical modeling for reflectivity

The measurement of reflected light intensity at the prism side is required for the sensing purpose of this SPR sensor, and the intensity of reflection of TM polarized light can be expressed as follows (Hossain et al., 2022; Maurya et al., 2015)

$$R_p = \left| r_p^2 \right| \tag{2}$$

$$r_p = \frac{(M_{11} + M_{12}q_N)n_1 - (M_{21} + M_{22}q_N)}{(M_{11} + M_{12}q_N)n_1 + (M_{21} + M_{22}q_N)} \tag{3}$$

Here, r_p represents the reflection coefficient for TM polarized incident light.

For a multilayer structure, the transfer matrix function, M_{ij} is given as follows (Maurya et al., 2015)

$$M_{ij} = \left(\prod_{k=2}^{N-1} M_k \right)_{ij} = \begin{pmatrix} M_{11} & M_{12} \\ M_{21} & M_{22} \end{pmatrix} \tag{4}$$

Table 1
Performance parameters of the proposed sensor at different wavelengths

RI Salinity (%)	Sensitivity (deg./RIU)					Detection accuracy (deg.$^{-1}$)					Quality factor (RIU^{-1})				
	633 nm	643.8 nm	690 nm	700 nm	720 nm	633 nm	643.8 nm	690 nm	700 nm	720 nm	633 nm	643.8 nm	690 nm	700 nm	720 nm
1.330 (0%)	–	–	–	–	–	–	–	–	–	–	–	–	–	–	
1.33175 (1%)	298	269	171.42	171	148.57	0.15	0.16	0.31	0.34	0.41	47	45	54.72	60	61.14
1.33266 (5%)	300	271	150.37	169	157.89	0.15	0.16	0.30	0.34	0.40	48	45	45.69	58	63.92
1.33357 (10%)	303	275	168.06	168	156.86	0.16	0.16	0.29	0.34	0.40	49	45	50.24	57	62.74
1.33447 (15%)	304	277	156.59	170	156.60	0.16	0.16	0.30	0.33	0.39	50	45	47.44	57	62.39
1.33538 (20%)	305	279	167.28	171	144.9	0.17	0.16	0.29	0.33	0.39	52	45	49.18	57	56.85
1.33629 (25%)	302	280	174.88	170	158.31	0.17	0.16	0.29	0.33	0.39	54	45	51.33	56	62.57
1.33699 (30%)	300	281	171.67	170	157.36	0.18	0.16	0.29	0.32	0.38	56	45	50.47	56	60.99

$$\text{with, } M_k = \begin{bmatrix} cos\beta_k & -(isin\beta_k)/q_k \\ -iq_k sin\beta_k & cos\beta_k \end{bmatrix}$$

$$\text{where, } q_k = \left(\frac{\mu_k}{\varepsilon_k}\right)^{1/2} cos\theta_k = \frac{\left(\varepsilon_k - n_1^2 sin^2\theta_1\right)^{1/2}}{\varepsilon_k} \tag{6}$$

$$\beta_k = \frac{2\pi}{\lambda} n_k cos\theta_k (z_k - z_{k-1}) = \frac{2\pi d_k}{\lambda}(\varepsilon_k - n_1^2 sin^2\theta_1)^{1/2} \tag{7}$$

2.3. Mathematical modeling of the performance parameters

The performance parameter of the proposed sensor is characterized on the basis of its sensitivity, quality factor, and detection accuracy . A good sensor is one that shows high sensitivity, high detection accuracy, and quality factor simultaneously (). The sensitivity of the sensor is defined as the shift of SPR angle ($\Delta\theta_{SPR}$) to the change in refractive index (RI) of the sensing medium (Δn_s) and its unit is deg./RIU.

Mathematically sensitivity (S) can be given by (Verma et al., 2015),

$$S = \frac{\Delta\theta_{SPR}}{\Delta n_s}(deg./RIU) \tag{8}$$

Detection accuracy (DA) can be determined for each refractive index of the sensing analyte and is given by (Verma et al., 2015);

$$DA = \frac{1}{\Delta\theta_{0.5}}\left(deg.^{-1}\right) \tag{9}$$

where $\Delta\theta_{0.5}$ is the spectral width of reflectance curve that's corresponds to 50% reflectivity. It is also known as full-width half maxima (FWHM). Quality factor (QF) depends on the sensitivity (S) and $\Delta\theta_{0.5}$ of reflectance curve, is given by (Verma et al., 2015),

$$QF = \frac{S}{\Delta\theta_{0.5}}\left(RIU^{-1}\right) \tag{10}$$

3. Results and discussions

The performance of the proposed sensor is evaluated and compared these evaluating parameters with the earlier reported works. The performance parameters are analyzed at different wavelength of the incident light. Reflectivity curves are plotted in Fig. 5 for wavelengths of 633 nm, 643.8 nm, 690 nm, 700 nm, and 720 nm. It is seen from the figures that maximum sensitivity is obtained at 633 nm wavelength. During the simulation, the RI of the sensing medium is taken from pure water (RI 1.330) to a change in salinity from 1% to 30%. For each wavelength and RI of the sensing medium, a dip of SPR curve occurs, and the reflectance intensity becomes minimum, the angle of incident light for which the reflectance intensity dip takes place is known as the SPR angle. Performance parameters at different wavelengths using the SPR curve are tabulated in Table 1. It's been observed in Table 1 that the maximum sensitivity obtained at 633 nm wavelength is 305 deg./RIU and minimum sensitivity is 298 deg./RIU, for 643.8 nm wavelength, 280 deg./RIU and 269 deg./RIU, for 690 nm wavelength 174.88 deg./RIU and 150.37 deg./RIU, for 700 nm wavelength, 171 deg./RIU and 168 deg./RIU, and for 720 nm wavelength, 158.31 deg./RIU and 148.57 deg./RIU respectively. It is also observed from Table 1 that sensitivity increases from 298 to 305 deg./RIU for 633 nm, 269 to 281 deg./RIU for 643.8 nm, 150.37 deg./RIU to 171.67 deg./RIU,168 to 171 deg./RIU for 700 nm, and 144.9 to 158.31 deg./RIU for 720 nm wavelength. Sensitivity increases beacuase a small change in salinity of seawater causes the position of resonance angle to shift to a higher value. In our work, maximum sensitivity of 305 deg./RIU is obtained at 633 nm wavelength, and sensitivity becomes minimum, 144.9 deg./RIU at 720 nm; this is due to the fact that change in SPR angle, $\Delta\theta_{SPR}$ is maximum 2.1° for 633 nm wavelength, and minimum 0.78° at 720 nm wavelength. The reduced effective light coupling to SPW results in low sensitivity at higher wavelengths (Qian et al., 2018). Fig. 6 displays the variation of sensitivity and DA with the change in RI of seawater. It can be observed from Fig. 6 that DA increases with the increasing of wavelength from 0.186 deg.$^{-1}$ at 633 nm to 0.41 deg.$^{-1}$ at 720 nm wavelength. At a higher wavelength, ohmic loss reduces, and thus detection accuracy improves as SPR curves become less broad (Nelson et al., 1999). The broadening of SPR curve is connected to the franckeite band gap which is less than 0.7 eV, and ohmic loss associated with metal (Ag). Refractive index of metals and dielectrics are connected to the wavelength of incident light. With an increase in wavelength, the real part of the complex refractive index of franckeite increases and imaginary part decreases, this decreasing imaginary part i.e. extinction coefficient causes smaller damping to the SPR curve and the curves become sharper for 700 nm wavelength as compared to 633 nm wavelength. In the SPR measurements, broadening of reflectivity curves is generally caused either by absorption at the used wavelength or by the roughness of the deposited film. The broadness of the SPR curves at 633 nm wavelength originates from the strong absorption of light at this wavelength. The less widening of SPR curve is attributed to the low absorption of light at 700 nm wavelength. Ohmic loss associated with metals depends on the wavelength of incident light. The reason of SPR curve being less widen, is attributed to the fact that at the higher wavelength, the ohmic loss in the metals is relatively low, thereby exhibiting sharper SPR curves (Pumera, 2011). The proposed sensor has been simulated for different wavelength of light i.e. 633 nm, 643.8 nm, 690 nm, 700 nm, and 720 nm and the simulated data are tabulated in Table 1. From Table 1, it is seen that with an increasing operating wavelength, DA, and QF increase, and it's been

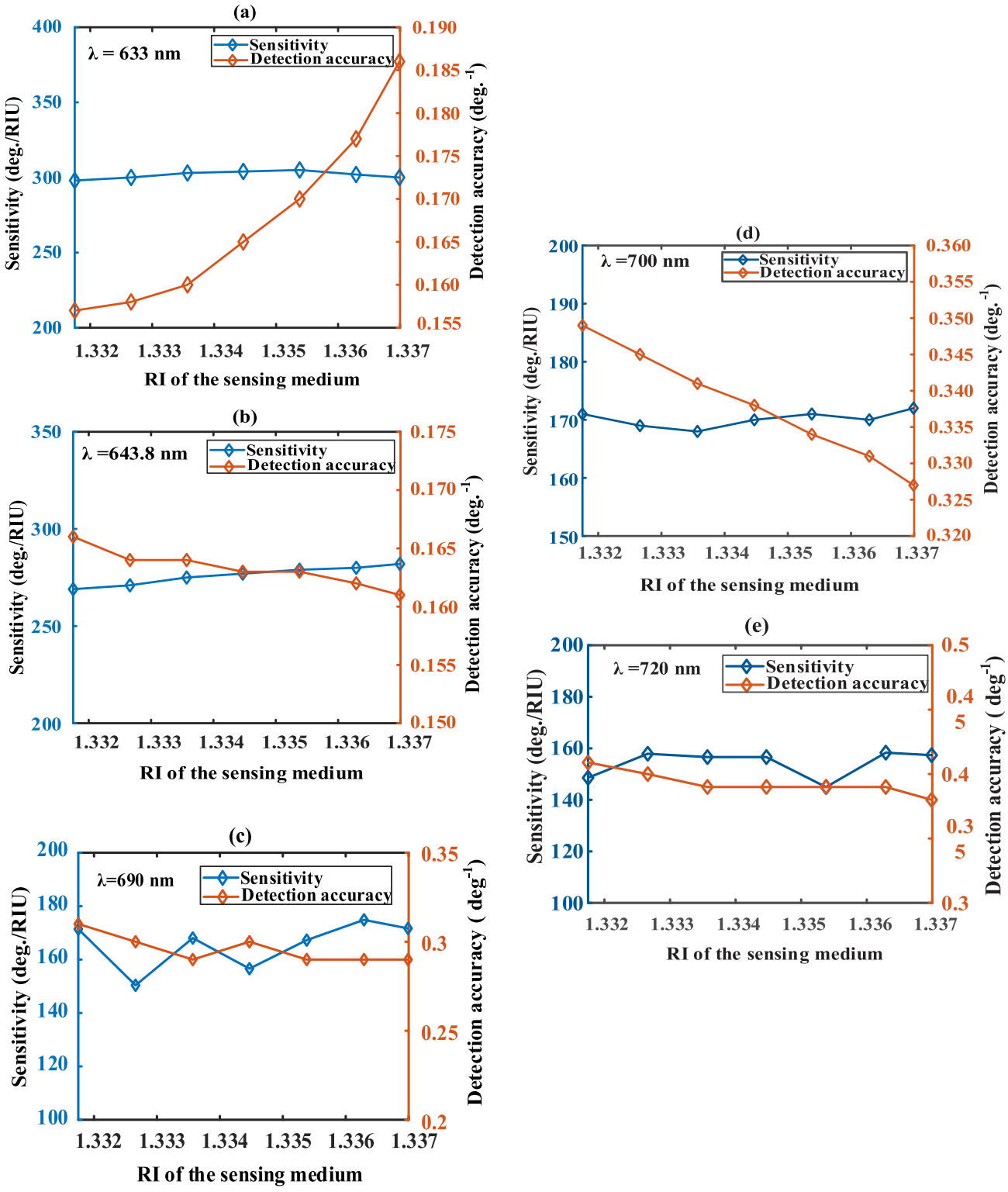

Fig. 6. Variation of sensitivity and DA with the variation of RI of the sensing medium at wavelengths, a) 633 nm, b) 643.8 nm, c) 690 nm, d) 700 nm, and e) 720 nm.

also observed that the sensitivity decreases. From Table 1, it is seen that, from 700 nm to 720 nm wavelength, there is a little improvement in QF and DA by sacrificing huge amount sensitivity in return of those improvements. Considering all the parameters, we can choose, 700 nm as an optimal wavelength of light as it provides an optimal performance.

Fig. 7 shows the variation of QF and sensitivity with the variation of RI of seawater at wavelengths of 633 nm, 643.8 nm, 690 nm, 700 nm, and 720 nm. It is observed that though the highest sensitivity of 305 deg./RIU is obtained at 633 nm, the highest QF is obtained at 700 nm wavelength. At lower wavelength, SPR curves become broader, resulting in lower QF, DA, and at higher wavelength curves becomes less broadening. For seawater RI of 1.33175–1.33699, QF varies from 47 to 52 RIU^{-1}, 45 RIU^{-1}, 47.44 RIU^{-1} to 54.72 RIU^{-1}, 56 to 60 RIU^{-1}, and 56.85 RIU^{-1} to 63.92 RIU^{-1} for 633 nm, 643.8 nm, 690 nm, 700 nm,

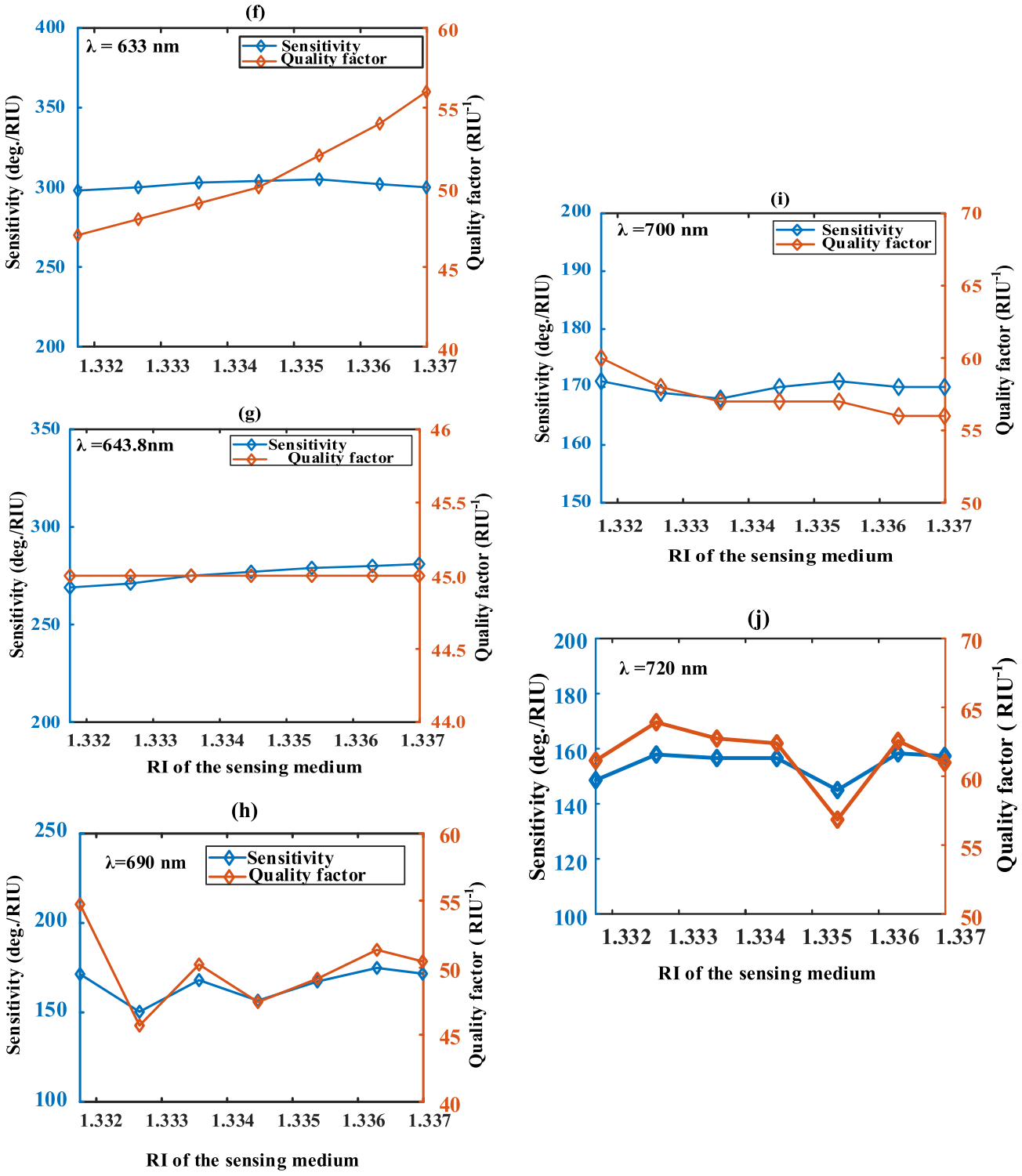

Fig. 7. Variation of sensitivity and QF with the variation of RI of sensing medium at wavelength f) 633 nm, g) 643.8 nm, h) 690 nm, i) 700 nm, and j) 720 nm.

and 720 nm respectively.

Fig. 8 displays sensitivity variation to the number of franckeite layers. The highest sensitivity is obtained with a single franckeite layer i. e. when L = 1. Fig. 9 displays the sensitivity of the proposed sensor with the variation of Si layer thickness. As shown in the figure, the optimized thickness for Si is 5 nm. With Si layer, maximum sensitivity obtained is 305 deg./RIU for 5 nm thickness of Si layer. Without Si layer, maximum sensitivity becomes 172 deg./RIU. Si layer enhances sensitivity as it increases the mobility of electrons in franckeite responsible for sensing analytes efficiently at its surface (Karki et al., 2021).

From Table 2, it is seen that a maximum sensitivity of 298 deg./RIU is obtained for 50 nm thickness of Ag layer with a reflectance intensity of 21.286 a.u. For a 45 nm of Ag, the sensitivity obtained is 274.28 deg./RIU and for 55 nm of Ag layer, the sensitivity obtained is 297.14 deg./RIU with a reflectance intensity of 41.9286 a.u for an analyte refractive index of 1.33175. With a 55 nm thickness of the Ag layer, the reflectance intensity becomes 55.59 a.u for an analyte refractive index of 1.33699. So, considering all this, we have chosen an optimized Ag layer thickness

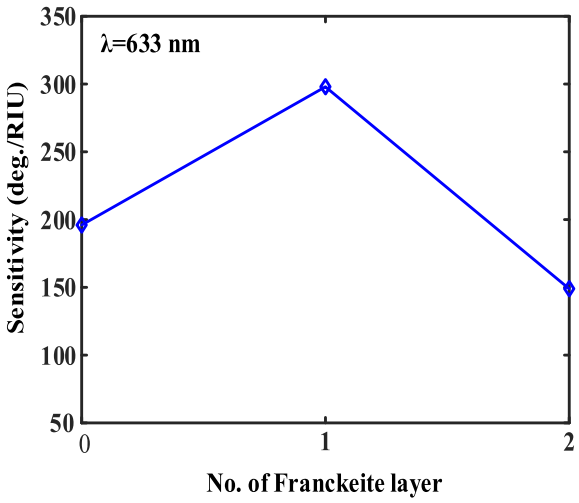

Fig. 8. Variation of sensitivity with the variation of no. of franckeite layer at 633 nm wavelength.

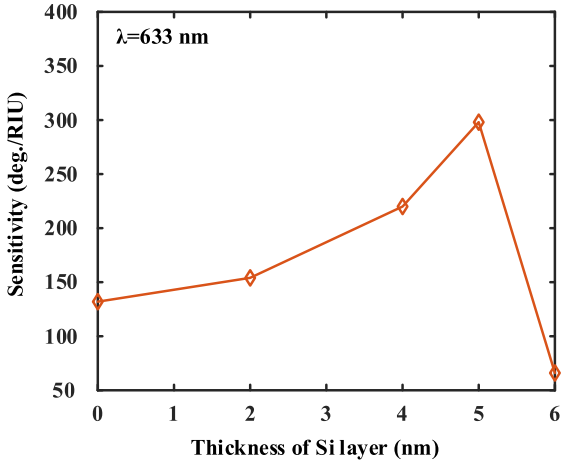

Fig. 9. Variation of sensitivity with the variation of thickness of Si layer at 633 nm wavelength.

Table 2
Optimization of Ag layer thickness.

Thickness	Sensitivity	Min. reflectacne (%) (a.u)
45	274.2857	3.4851
50	298	21.2860
55	297.14	41.9238

of 50 nm as it provides optimized performance. In Fig. 10, we have shown sensitivity versus thickness curves for the Ag layer.

In the proposed work, performance parameters are calculated using simulation data obtained from FEM based 'COMSOL MULTIPHYSICS' platform. The performance parameters can also be calculated using transfer matrix method (TMM). In Table 3, a comparison of performance parameters using FEM, and TMM is provided.

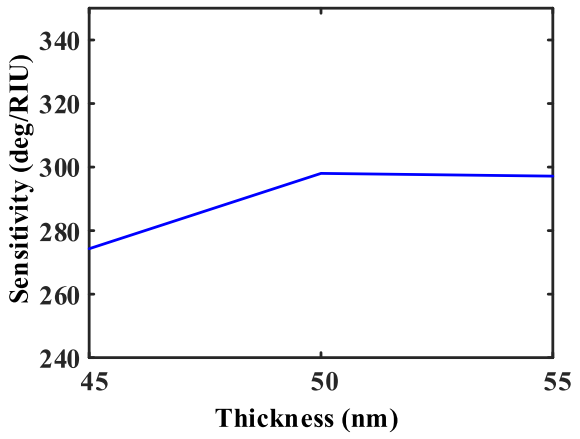

Fig. 10. Sensitivity with the variation of Ag layer.

Table 3
Comparison of the performance parameters using different numerical methods.

SL no.	Methods	Parameters			Ref.
		S (deg./RIU)	DA ($deg.^{-1}$)	QF (RIU^{-1})	
1	TMM	194	0.091	34.22	(Rahman et al., 2020)
2	TMM	208	–	17.33	(Srivastava and Prajapati, 2020)
3	TMM	143.08	0.165	23.72	(Raikwar et al., 2020)
4	FEM	305	0.410	63.92	In this work

Table 4 shows the comparison of the proposed work with the earlier reported works. From the table it is seen that on the basis of performance, the designed sensors outperforms previously reported works.

4. Conclusion

This work describes a highly sensitive prism-coupled SPR based optical salinity sensor that is simulated and analyzed theoretically utilizing franckeite nanosheets, a newly developed 2D material. The designed sensor has been optimized in terms of thicknesses of franckneite, Ag, and Si layer. To achieve the best possible performance *i. e.* sensitivity, detection accuracy, and quality factor, the sensor is designed and simulated at different wavelengths of 633 nm, 643.8 nm, 640 nm, 700 nm, and 720 nm. Here, the sensor is designed to measure the salinity of seawater. The proposed sensor exhibits enhanced sensitivity, quality factor, and detection accuracy than the previously reported works. The sensitivity of the conventional SPR sensor enhances with the addition of Si and franckeite layer as the absorption efficiency of franckeite is higher, and the Si enhances the mobility of the electrons in franckeite responsible for efficient sensing of analytes in the sensing medium. The optimized sensor provides a maximum sensitivity of 305 deg./RIU, detection accuracy of 0.41 $deg.^{-1}$, and quality facor of 63.92 RIU^{-1}. Performance parameters i.e. sensitivity, detection accuracy, and quality factor are enhanced to a great extent in comparison with the earlier reported works. The raised sensor could be accomplished by utilizing the available fabrication technologies. As the proposed sensor provides promising results, this could be applied to measure the salinity of seawater.

Table 4
Comparison with earlier reported work.

Reference	Wavelength (nm)	Structure	Sensitivity (deg./RIU)	Detection accuracy (deg.$^{-1}$)	Quality factor (RIU^{-1})
(Raikwar et al., 2020)	632.8 nm	Au-GO	143.08	0.165	23.72
Proposed work	633	Ag-Si-Franckeite	305	0.18	56
	643.8		281	0.16	45
	690		174.88	0.31	51.33
	700		171	0.34	60
	720		158.31	0.41	63.92

CRediT authorship contribution statement

Belal Hossain: Conceptualization, Methodology, Software, Writing – original draft. **Alok Kumar Paul:** Formal analysis, Investigation, Writing – review & editing, Supervision. **Md. Arefin Islam:** Software. **Md. Faruk Hossain:** Investigation, Supervision. **Md. Mahabubur Rahman:** Writing – review & editing.

Declaration of Competing Interest

The authors declare that they have no known competing financial interests or personal relationships that could have appeared to influence the work reported in this paper.

References

Adamo, F., Attivissimo, F., Guarnieri Calo Carducci, C., Lanzolla, A.M.L., 2015. A smart sensor network for sea water quality monitoring. IEEE Sens. J. 15 (5), 2514–2522. https://doi.org/10.1109/JSEN.2014.2360816.

Austin, R. W, & Halikas, G. (1976). The index of refraction of seawater. *UC San Diego: Library – Scripps Digital Collection*. Retrieved from https://escholarship.org/uc/item/8px2019m.

Bae, S., Kim, H., Lee, Y., Xu, X., Park, J.-S., Zheng, Y.i., Balakrishnan, J., Lei, T., Ri Kim, H., Song, Y.I., Kim, Y.-J., Kim, K.S., Özyilmaz, B., Ahn, J.-H., Hong, B.H., Iijima, S., 2010. Roll-to-roll production of 30-inch graphene films for transparent electrodes. Nat. Nanotechnol. 5 (8), 574–578. https://doi.org/10.1038/nnano.2010.132.

Baker, R.W., 2012. Membrane Technology and Applications. John Wiley & Sons doi: 10.1002/9781118359686.

Boehm, J., François, A., Ebendorff-Heidepriem, H., Monro, T.M., 2011. Chemical deposition of silver for the fabrication of surface plasmon microstructured optical fibre sensors. Plasmonics 6 (1), 133–136. https://doi.org/10.1007/s11468-010-9178-z.

Brahmachari, K., Ray, M., 2013. Effect of prism material on design of surface plasmon resonance sensor by admittance loci method. Front. Optoelectron. 6 (2), 185–193. https://doi.org/10.1007/s12200-013-0313-2.

Dutta, S., Huang, S.Y., Chen, C., Chen, J.E., Alothman, Z.A., Yamauchi, Y., Wu, K.C.W., 2016. Cellulose framework directed construction of hierarchically porous carbons offering high-performance capacitive deionization of brackish water. ACS Sustain Chem. Eng. 4 (4), 1885–1893. https://doi.org/10.1021/ja4019572.

Elimelech, M., 2006. The global challenge for adequate and safe water. J Water Supply Res Technol AQUA 55 (1), 3–10. https://doi.org/10.2166/aqua.2005.064.

Etesami, H., & Noori, F. (2019). Soil salinity as a challenge for sustainable agriculture and bacterial-mediated alleviation of salinity stress in crop plants. In *Saline soil-based agriculture by halotolerant microorganisms* (pp. 1-22). Springer, Singapore, doi: 10.1007/978-981-13-8335-9_1.

Gan, S., Zhao, Y., Dai, X., Xiang, Y., 2019. Sensitivity enhancement of surface plasmon resonance sensors with 2D franckeite nanosheets. Results Phys. 13, 102320. https://doi.org/10.1016/j.rinp.2019.102320.

Gant, P., Ghasemi, F., Maeso, D., Munuera, C., López-Elvira, E., Frisenda, R., De Lara, D. P., Rubio-Bollinger, G., Garcia-Hernandez, M., Castellanos-Gomez, A., 2017. Optical contrast and refractive index of natural van der Waals heterostructure nanosheets of franckeite. Beilstein J. Nanotechnol. 8, 2357–2362. https://doi.org/10.3762/bjnano.8.235.

Garcia-Basabe, Y., Steinberg, D., Daminelli, L.M., Mendoza, C.D., de Souza, E.T., Vicentin, F.C., Larrudé, D.G., 2021. Charge-transfer dynamics in van der Waals heterojunctions formed by thiophene-based semiconductor polymers and exfoliated franckeite investigated from resonantly core-excited electrons. PCCP 23 (31), 16795–16805. https://doi.org/10.1039/D1CP01694F.

Ghosh, S., Ray, M., 2015. Analysis of silicon based surface plasmon resonance sensors with different amino acids. Silicon 7 (4), 313–322. https://doi.org/10.1007/s12633-015-9293-8.

Homola, J., Yee, S.S., Gauglitz, G., 1999. Surface plasmon resonance sensors. Sens. Actuat. B 54 (1–2), 3–15. https://doi.org/10.1016/S0925-4005(98)00321-9.

Hossain, B., Paul, A.K., Islam, M.A., Rahman, M.M., Sarkar, A.K., Abdulrazak, L.F., 2022. A highly sensitive surface plasmon resonance biosensor using SnSe allotrope and heterostructure of BlueP/MoS2 for cancerous cell detection. Optik 252, 168506. https://doi.org/10.1016/j.ijleo.2021.168506.

Y. Jia, Z. Li, H. Wang, M. Saeed, and H. Cai, "Sensitivity enhancement of a surface plasmon resonance sensor with platinum diselenide," Sensors (Switzerland), vol. 20, no. 1, 2020, doi: 10.3390/s20010131.

Jia, Y., Li, Z., Wang, H., Saeed, M., Cai, H., 2020. Sensitivity enhancement of a surface plasmon resonance sensor with platinum diselenide. Sensors 20 (1), 131. https://doi.org/10.3390/s20010131.

Karki, B., Sharma, S., Singh, Y., Pal, A., 2021. Sensitivity enhancement of surface plasmon resonance biosensor with 2-D franckeite nanosheets. Plasmonics 1–8. https://doi.org/10.1007/s11468-021-01495-6.

Kumar, R., Pal, S., Verma, A., Prajapati, Y.K., Saini, J.P., 2020. Effect of silicon on sensitivity of SPR biosensor using hybrid nanostructure of black phosphorus and MXene. Superlatt. Microstruct. 145, 106591. https://doi.org/10.1016/j.spmi.2020.106591.

Kusko, M., 2012. Design of low cost surface plasmon resonance sensor Vol. 1, 251–254. https://doi.org/10.1109/SMICND.2012.6400720.

Lee, A., Elam, J.W., Darling, S.B., 2016. Membrane materials for water purification: design, development, and application. Environ. Sci. Water Res. Technol. 2 (1), 17–42. https://doi.org/10.1039/C5EW00159E.

Matsumura, H., Tachibana, H., 1985. Amorphous silicon produced by a new thermal chemical vapor deposition method using intermediate species SiF_2. Appl. Phys. Lett. 47 (8), 833–835. https://doi.org/10.1063/1.96000.

Maurya, J.B., Prajapati, Y.K., Singh, V., Saini, J.P., Tripathi, R., 2015. Performance of graphene–MoS 2 based surface plasmon resonance sensor using silicon layer. Opt. Quant. Electron. 47 (11), 3599–3611. https://doi.org/10.1007/s11082-015-0233-z.

Molina-Mendoza, A.J., Giovanelli, E., Paz, W.S., Niño, M.A., Island, J.O., Evangeli, C., Aballe, L., Foerster, M., van der Zant, H.S.J., Rubio-Bollinger, G., Agraït, N., Palacios, J.J., Pérez, E.M., Castellanos-Gomez, A., 2017. Franckeite as a naturally occurring van der Waals heterostructure. Nat. Commun. 8 (1) https://doi.org/10.1038/ncomms14409.

Nelson, B.P., Frutos, A.G., Brockman, J.M., Corn, R.M., 1999. Near-infrared surface plasmon resonance measurements of ultrathin films. 1. Angle shift and SPR imaging experiments. Anal. Chem. 71 (18), 3928–3934.

Oki, T., Kanae, S., 2006. Global hydrological cycles and world water resources. Science 313 (5790), 1068–1072. https://doi.org/10.1126/science.1128845.

Ouyang, Q., Zeng, S., Jiang, L.i., Hong, L., Xu, G., Dinh, X.-Q., Qian, J., He, S., Qu, J., Coquet, P., Yong, K.-T., 2016. Sensitivity enhancement of transition metal dichalcogenides/silicon nanostructure-based surface plasmon resonance biosensor. Sci. Rep. 6 (1) https://doi.org/10.1038/srep28190.

Pal, A., Bisht, S., Sharma, A., Panwar, B. S., Bhayana, D. A., Sharma, S., & Srivastava, S. C. (2021, April). Prism Based Surface Plasmon Resonance Biosensor for Biomedical Applications. In ICOL-2019: Proceedings of the International Conference on Optics and Electro-Optics, Dehradun, India (pp. 437-440). Springer Singapore, doi: 10.1007/978-981-15-9259-1_100.

Pal, S., Verma, A., Prajapati, Y.K., Saini, J.P., 2020. Sensitive detection using heterostructure of black phosphorus, transition metal di-chalcogenides and MXene in SPR sensor. Appl. Phys. A Mater. Sci. Process. 126 (10), 1–10. https://doi.org/10.1007/s00339-020-03998-1.

Peng, Q., Wang, Z., Sa, B., Wu, B., Sun, Z., 2016. Electronic structures and enhanced optical properties of blue phosphorene/transition metal dichalcogenides van der Waals heterostructures. Sci. Rep. 6, 2–11. https://doi.org/10.1038/srep31994.

Pumera, M., 2011. Graphene in biosensing. Mater. Today 14 (7-8), 308–315. https://doi.org/10.1016/S1369-7021(11)70160-2.

Qian, Y., Zhao, Y., Wu, Q.L., Yang, Y., 2018. Review of salinity measurement technology based on optical fiber sensor. Sens. Actuators, B 260, 86–105. https://doi.org/10.1016/j.optlastec.2021.107543.

Rahman, M.M., Rana, M.M., Rahman, M.S., Anower, M.S., Mollah, M.A., Paul, A.K., 2020. Sensitivity enhancement of SPR biosensors employing heterostructure of PtSe2 and 2D materials. Opt. Mater. 107, 110123. https://doi.org/10.1016/j.optmat.2020.110123.

Raikwar, S., Prajapati, Y.K., Srivastava, D.K., Saini, J.P., 2020. Graphene oxide based SPR sensor for sensing of sea water concentration. Results Opt. 1, 100011. https://doi.org/10.1016/j.rio.2020.100011.

Ray, K., Yore, A.E., Mou, T., Jha, S., Smithe, K.K.H., Wang, B., Pop, E., Newaz, A.K.M., 2017. Photoresponse of natural van der Waals heterostructures. ACS Nano 11 (6), 6024–6030. https://doi.org/10.1021/acsnano.7b0191810.1021/acsnano.7b01918.s001.

Rikta, K.A., Anower, M.S., Rahman, M.S., Rahman, M.M., 2021. SPR biosensor using SnSe-phosphorene heterostructure. Sens. Bio-Sens. Res. 33, 100442. https://doi.org/10.1016/j.sbsr.2021.100442.

Rosen, J.S., 1947. The refractive indices of alcohol, water, and their mixtures at high pressures. JOSA 37 (11), 932–938. https://doi.org/10.1364/JOSA.37.000932.

SCOR/IAPSO Working Group 127 on Thermodynamics and Equation of State of Seawater, Meetings 6–11 May 2007, Reggio/Calabria, Italy.

Shannon, M.A., Bohn, P.W., Elimelech, M., Georgiadis, J.G., Mariñas, B.J., Mayes, A.M., 2009. Science and technology for water purification in the coming decades. In: Rodgers, P. (Ed.), Nanoscience and Technology: A Collection of Reviews from Nature Journals. Co-Published with Macmillan Publishers Ltd, UK, pp. 337–346. https://doi.org/10.1142/9789814287005_0035.

Sharma, A.K., Pandey, A.K., 2018. Blue phosphorene/MoS 2 heterostructure based SPR sensor with enhanced sensitivity. IEEE Photon. Technol. Lett. 30 (7), 595–598. https://doi.org/10.1109/LPT.2018.2803747.

Srivastava, A., Prajapati, Y.K., 2019. Performance analysis of silicon and blue phosphorene/MoS2 hetero-structure based SPR sensor. Photonic Sensors 9 (3), 284–292. https://doi.org/10.1007/s13320-019-0533-1.

Srivastava, A., Prajapati, Y.K., 2020. Effect of sulfosalt and polymers on performance parameter of SPR biosensor. Opt. Quant. Electron. 52 (10) https://doi.org/10.1007/s11082-020-02545-9.

Velický, M., Toth, P.S., Rakowski, A.M., Rooney, A.P., Kozikov, A., Woods, C.R., Mishchenko, A., Fumagalli, L., Yin, J., Zólyomi, V., Georgiou, T., Haigh, S.J., Novoselov, K.S., Dryfe, R.A.W., 2017. Exfoliation of natural van der Waals heterostructures to a single unit cell thickness. Nat. Commun. 8 (1) https://doi.org/10.1038/ncomms14410.

Verma, A., Prakash, A., Tripathi, R., 2015. Sensitivity enhancement of surface plasmon resonance biosensor using graphene and air gap. Opt. Commun. 357, 106–112. https://doi.org/10.1016/j.optcom.2015.08.076.

Wang, M., Xu, X., Tang, J., Hou, S., Hossain, M.S.A., Pan, L., Yamauchi, Y., 2017. High performance capacitive deionization electrodes based on ultrathin nitrogen-doped carbon/graphene nano-sandwiches. Chem. Commun. 53 (78), 10784–10787. https://doi.org/10.1039/C7CC05673G.

Xia, L., Yin, S., Gao, H., Deng, Q., Du, C., 2011. Sensitivity enhancement for surface plasmon resonance imaging biosensor by utilizing gold–silver bimetallic film configuration. Plasmonics 6 (2), 245–250. https://doi.org/10.1007/s11468-010-9195-y.

Xu, X., Allah, A.E., Wang, C., Tan, H., Farghali, A.A., Khedr, M.H., Malgras, V., Yang, T., Yamauchi, Y., 2019. Capacitive deionization using nitrogen-doped mesostructured carbons for highly efficient brackish water desalination. Chem. Eng. J. 362, 887–896. https://doi.org/10.1016/j.cej.2019.01.098.

Zhang, X., Meng, F., Christianson, J.R., Arroyo-Torres, C., Lukowski, M.A., Liang, D., Schmidt, J.R., Jin, S., 2014. Vertical heterostructures of layered metal chalcogenides by van der Waals epitaxy. Nano Lett. 14 (6), 3047–3054. https://doi.org/10.1021/nl501000k.

Zhu, C., Zeng, Z., Li, H., Li, F., Fan, C., Zhang, H., 2013. Single-layer MoS2-based nanoprobes for homogeneous detection of biomolecules. J. Am. Chem. Soc. 135 (16), 5998–6001. https://doi.org/10.1021/ja4019572.